Rickettsia parkeri Sca2 promotes dissemination in an intradermal infection mouse model

Thomas P. Burke[1]*, Cuong J. Tran[1,2], Patrik Engström[1], Dustin R. Glasner[2,3], Diego A. Espinosa[2,4], Eva Harris[2], Matthew D. Welch[1]*

[1]Department of Molecular and Cell Biology, University of California, Berkeley, Berkeley, CA, USA

[2]Division of Infectious Disease and Vaccinology, School of Public Health, University of California, Berkeley, Berkeley, CA, USA

[3]Current address: Department of Laboratory Medicine, University of California, San Francisco, San Francisco, CA, USA

[4]Current address: Metagenomi, Emeryville, CA, USA

*email: tburke@berkeley.edu; welch@berkeley.edu

Abstract

Arthropod-borne pathogens cause severe human and animal diseases worldwide; however, current animal models are often inadequate in recapitulating key features of infection. Here, we report an intradermal infection model for *Rickettsia parkeri*, which causes eschar-associated spotted fever rickettsiosis in humans. We show that infection of mice lacking both interferon receptors (*Ifnar*$^{-/-}$*Ifngr*$^{-/-}$) with *R. parkeri* causes skin lesion formation similar to human eschars and disseminated disease with as few as 10 bacteria. Using this model, we found that the actin-based motility protein Sca2 is dispensable for *R. parkeri* survival in organs but is required for *R. parkeri* dissemination from the skin to peripheral tissues and for causing lethal disease. We also found that immunizing mice with *sca2* and *ompB* mutant *R. parkeri* protects against subsequent rechallenge with wild-type bacteria. This study characterizes a mouse model that mimics aspects of human rickettsial disease and reveals a pathogenic role for the *R. parkeri* actin-based motility protein Sca2 in dissemination.

Introduction

Obligate cytosolic bacterial pathogens in the family Rickettsiaceae are a diverse group of arthropod-borne microbes that cause severe human disease worldwide, including spotted fever, scrub typhus, and typhus[1–3]. Many critical aspects of disease caused by obligate cytosolic bacterial pathogens remain unknown, as there are few model pathogens that can be handled under biosafety level 2 (BSL2) conditions with corresponding mouse models that recapitulate key features of human disease[4–6]. One model that has emerged to study the pathogenesis of spotted fever group *Rickettsia* species is *Rickettsia parkeri*, which causes mild eschar-associated spotted fever disease in humans[7]. *R. parkeri* is genetically similar to the more virulent human pathogens *R. rickettsii* and *R. conorii*[8,9], and it can be handled under BSL2 conditions. Moreover, mutants can be generated using transposon mutagenesis[10,11]. However, current mouse models fail to recapitulate symptoms of human disease, limiting investigations into *R. parkeri* pathogenesis.

Small rodents including mice are natural reservoirs for *R. parkeri*[12–15]. However, inbred mice including C57BL/6 and BALB/c develop no or limited skin lesions upon intradermal (i.d.) infection[4]. C3H/HEJ mice, which harbor a mutation in the gene encoding Toll-like receptor 4 (TLR4), the receptor for extracellular lipopolysaccharide (LPS), have been proposed as models for *R. parkeri*, yet they do not develop disseminated disease and only develop minor skin lesions upon i.d. inoculation[4]. C57BL/6 mice have also been proposed as models for *R. parkeri* upon intravenous (i.v.) delivery of 10^8 bacteria[16]. However, this dose is substantially higher than the number of *R. parkeri* found in tick saliva or tick salivary glands[17], and considerable effort is required to generate and concentrate this number of bacteria. An improved mouse model to investigate *R. parkeri* would greatly increase the ability to investigate virulence mechanisms, the host response to infection, human rickettsial disease, and propagation of tick-borne pathogens in animal reservoirs.

One remarkable mechanism of pathogenesis exhibited by cytosolic bacterial pathogens is their ability to manipulate the host cell actin cytoskeleton to propel themselves throughout the cell via actin-based motility. Highly divergent cytosolic bacterial pathogens including *Rickettsia, Listeria, Burkholderia, Mycobacterium,* and *Shigella* species undergo actin-based motility, facilitating cell-to-cell

spread[18,19]. Among the factors that mediate actin-based motility, the *L. monocytogenes* actin-based motility factor ActA is one of the best understood. ActA enables *L. monocytogenes* to spread from cell to cell[18,19], escape antimicrobial autophagy[20–23], proliferate in mouse organs after i.v. infection[24,25], and cause lethal disease in mice[26,27]. The pathogenic roles for actin-based motility factors in many other cytosolic bacterial pathogens, however, remain poorly understood. *R. parkeri* actin-based motility differs from that of other pathogens in that it occurs in two phases, one that requires the RickA protein[10,28] and the other that requires the Sca2 protein[10,29]. Only Sca2 is required for efficient cell-to-cell spread *in vitro*[10,29], although it is not required for replication in epithelial cells[10,29,30] or avoiding autophagy recognition[31]. Although *sca2* mutant *R. rickettsii* elicit reduced fever in guinea pigs as compared with wild-type (WT) *R. rickettsii*[29], the explanation for reduced fever and the pathogenic role for Sca2 *in vivo* remains unclear. Additionally, Sca2 is not essential for dissemination of *R. parkeri* within the tick vector[32]. Therefore, it remains unresolved how Sca2 enhances rickettsial pathogenesis or fitness.

In a recent investigation of the relationship between *R. parkeri* and interferons (IFNs), ubiquitous signaling molecules of the innate immune system that mobilize the cytosol to an antimicrobial state, we observed that mice lacking the genes encoding the receptors for type I interferon (*Ifnar*) and IFN-γ (*Ifngr*) succumb to i.v. infection by *R. parkeri*[33]. Here, we use these IFN receptor-deficient mice to examine the effects of i.d. inoculation of *R. parkeri*, mimicking the natural route of infection. We observe severe skin lesion formation, similar to human infection, as well as disseminated lethal disease with as few as 10 bacteria. Using this infection model, we reveal a role for Sca2 in *R. parkeri* dissemination. Finally, we demonstrate that immunization with *sca2* and other mutant *R. parkeri* can protect IFN receptor-deficient mice against subsequent challenge with WT bacteria. This work establishes a mouse model to investigate numerous aspects of *Rickettsia* pathogenesis, including eschar formation, virulence factors, and immunity.

Results

I.d. infection of *Ifnar*$^{-/-}$*Ifngr*$^{-/-}$ mice causes lethal disease and skin lesions that are grossly similar to human eschars.

Although i.v. delivery can recapitulate an immediate systemic disease for many pathogens, it does not mimic the natural route of infection for tick-borne pathogens. In contrast, i.d. delivery better mimics the natural route of infection and allows for investigations into dissemination from the initial infection site to peripheral organs. We therefore sought to develop an i.d. murine infection model to better recapitulate the natural route of tick-borne *R. parkeri* infection. WT, *Tlr4*$^{-/-}$, *Ifnar*$^{-/-}$, *Ifngr*$^{-/-}$, and *Ifnar*$^{-/-}$*Ifngr*$^{-/-}$ C57BL/6J mice, as well as outbred CD-1 mice, were infected i.d. with 10^7 WT *R. parkeri* and monitored over time. No or minor dermal lesions appeared at the site of infection in WT, *Tlr4*$^{-/-}$, *Ifnar*$^{-/-}$, or *Ifngr*$^{-/-}$ C57BL/6J mice or CD-1 mice. In contrast, double mutant *Ifnar*$^{-/-}$*Ifngr*$^{-/-}$ C57BL/6J mice developed large necrotic lesions (**Fig. 1a,b, Extended Data Fig. 1a**) similar to human eschars (**Fig. 1c**). In some cases, tails of *Ifnar*$^{-/-}$*Ifngr*$^{-/-}$ or *Ifngr*$^{-/-}$ mutant mice became inflamed after i.d. or i.v. infection (**Extended Data Fig. 1b**). These findings demonstrate that interferons redundantly control disease caused by *R. parkeri* in the skin and that i.d. infection of *Ifnar*$^{-/-}$*Ifngr*$^{-/-}$ mice recapitulates the hallmark symptom of human disease caused by *R. parkeri*.

Our previous observations using the i.v. route revealed dose-dependent lethality in *Ifnar*$^{-/-}$*Ifngr*$^{-/-}$ mice, with 10^7 *R. parkeri* eliciting 100% lethality and 10^5 *R. parkeri* eliciting no lethality[33]. *R. parkeri* are present in tick saliva at a concentration of approximately 10^4 per 1 μl, and approximately 10^7 *R. parkeri* are found in tick salivary glands[17]. However, the number of bacteria delivered from tick infestation likely varies depending on many factors, and we therefore sought to examine the effects of different doses of *R. parkeri* upon i.d. infection of *Ifnar*$^{-/-}$*Ifngr*$^{-/-}$ mice. We observed skin lesion formation at all infectious doses, from 10^7 to 10 bacteria (**Fig. 1d**), suggesting that i.d. infection of *Ifnar*$^{-/-}$*Ifngr*$^{-/-}$ mice elicits lesions with doses similar to what is delivered by tick infestation.

We next sought to quantitatively evaluate the effects of i.d. infection by monitoring animal weight, body temperature, the degree of lesion formation, and lethality. Intradermally-infected *Ifnar*$^{-/-}$*Ifngr*$^{-/-}$ mice lost significant body weight (**Fig. 2a; Extended Data Fig. 2a**) and body temperature (**Fig. 2b**; animals

were euthanized when body temperature fell below 90° F) as compared with WT mice, whereas infected *Tlr4*$^{-/-}$, *Ifnar*$^{-/-}$, *Ifngr*$^{-/-}$ mice did not. To evaluate lesion severity, we scored lesions upon infection with different doses of *R. parkeri*. Whereas 10^7 bacteria elicited similar responses as 10^5, 10^4, 10^3, and 10^2 bacteria (**Fig. 2c**), lesions were less severe when mice were infected with 10^1 bacteria compared with 10^7 bacteria. If mice survived, lesions healed over the course of approximately 15-40 days post infection (d.p.i.) at all doses (**Extended Data Fig. 2b**).

To investigate whether i.d. infection by *R. parkeri* caused lethal disease, we monitored mouse survival over time. Upon i.d. delivery of 10^7 *R. parkeri,* 8 of 12 *Ifnar*$^{-/-}$*Ifngr*$^{-/-}$ mice exhibited lethargy, paralysis, or body temperatures below 90° F, at which point they were euthanized (**Fig. 1e**), whereas delivery of the same dose of bacteria to WT and single mutant mice did not elicit lesions and all survived (**Fig. 2d**). Lower doses of *R. parkeri* also elicited body weight loss (**Fig. 2a**), body temperature loss (**Extended Data Fig. 2c**), and lethal disease (**Fig. 2d**) in *Ifnar*$^{-/-}$*Ifngr*$^{-/-}$ mice. The cause of lethality in this model remains unclear and will require further investigation. Nevertheless, these findings reveal that i.d. infection can cause lethal disease in *Ifnar*$^{-/-}$*Ifngr*$^{-/-}$ mice with ~10,000-fold lower dose of bacteria than i.v. infection.

It remained unclear whether i.d. infection could also be used to model dissemination from the skin to peripheral organs. We therefore evaluated bacterial burdens in spleens and livers of WT and *Ifnar*$^{-/-}$*Ifngr*$^{-/-}$ mice at 5 d.p.i. by measuring *R. parkeri* plaque-forming units (p.f.u.). Bacteria were not recoverable from spleens and livers of intradermally-infected WT mice, suggesting that they did not disseminate from the skin to peripheral organs in high numbers (**Fig. 2e**). In contrast, bacteria were recovered from spleens and livers of intradermally-infected *Ifnar*$^{-/-}$*Ifngr*$^{-/-}$ mice at 5 d.p.i. (**Fig. 2e**). This demonstrates that i.d. infection of *Ifnar*$^{-/-}$*Ifngr*$^{-/-}$ mice with *R. parkeri* causes systemic infection and can be used as a model for dissemination from the skin to peripheral tissues.

R. parkeri **Sca2 is required for lethal disease in** ***Ifnar***$^{-/-}$***Ifngr***$^{-/-}$ **mice.**

Sca2 mediates actin-based motility in rickettsial pathogens; however, its contribution to virulence *in vivo* remains unclear. We therefore examined if i.v. and i.d. infections of WT and *Ifnar*$^{-/-}$*Ifngr*$^{-/-}$ mice

could reveal a pathogenic role for *R. parkeri* Sca2. Upon i.v. infection with 5 x 10^6 bacteria (**Fig. 3a**) or 10^7 bacteria (**Fig. 3b)**, we observed that *sca2*::Tn mutant *R. parkeri* caused reduced lethality compared to WT bacteria. Similarly, i.d. infection with *sca2*::Tn mutant bacteria elicited significantly less lethality (**Fig. 3c**) and weight loss (**Fig. 3d**) as compared to WT bacteria and no severe temperature loss (**Extended Data Fig. 3a**). Although we sought to evaluate infection using a *sca2* complement strain of *R. parkeri,* our attempts to generate such a strain were unsuccessful. As an alternative strategy, we examined whether the transposon insertion itself had an effect on *R. parkeri* survival *in vivo*. We evaluated infection of an *R. parkeri* strain that harbors a transposon insertion in *MC1_RS08740* (previously annotated as *MC1_05535*), which has no known role in virulence[31]. I.v. infection with *MC1_RS08740*::Tn *R. parkeri* caused lethality to a similar degree as WT *R. parkeri* (**Fig. 3a**), demonstrating that the transposon likely does not significantly impact *R. parkeri* fitness *in vivo*. Together, these findings suggest that the actin-based motility factor Sca2 is required for causing lethal disease in *Ifnar*$^{-/-}$*Ifngr*$^{-/-}$ mice.

WT and *sca2*::Tn *R. parkeri* elicit similar lesion formation and vascular damage in the skin.

We next examined whether Sca2 facilitates *R. parkeri* dissemination throughout the skin and whether Sca2 is required for lesion formation. Unexpectedly, upon i.d. inoculation, *Ifnar*$^{-/-}$*Ifngr*$^{-}$ mice infected with *sca2*::Tn mutant bacteria developed skin lesions that were of similar severity to lesions caused by WT *R. parkeri*; however, the lesions elicited by *sca2* mutant bacteria appeared significantly earlier than lesions caused by WT bacteria (**Fig. 3e**). Further examinations will be required to better evaluate this observation; however, it may suggest that actin-based motility enables *R. parkeri* to avoid a rapid onset of inflammation in the skin. To evaluate *R. parkeri* dissemination within the skin, we used a fluorescence-based assay that measures vascular damage as a proxy for pathogen dissemination[34]. Mice were intradermally infected with WT and *sca2*::Tn *R. parkeri*. At 5 d.p.i., fluorescent dextran was intravenously delivered, and fluorescence was measured at the infection site (**Fig. 3f**, representative small black circle) and in the surrounding area (**Fig. 3f**, representative large black circle). No significant differences were observed when comparing WT and *sca2*::Tn *R. parkeri* infections in *Ifnar*$^{-/-}$*Ifngr*$^{-/-}$ mice

using an infectious dose of 10^7 *R. parkeri* in the larger surrounding area (**Fig. 3g**) or at the site of infection (**Extended Data Fig. 4a**). Similar results were observed upon infection with 10^6 or 10^5 bacteria (**Extended Data Fig. 4b,c**). However, significantly more fluorescence was observed in the skin of infected *Ifnar*$^{-/-}$*Ifngr*$^{-/-}$ mice as compared to WT mice (**Fig. 3g**), demonstrating that interferons protect against increased vascular permeability during *R. parkeri* infection. Together, the gross pathological analysis and fluorescence-based assay suggest that Sca2 likely does not significantly enhance *R. parkeri* dissemination in the skin during i.d. infection of *Ifnar*$^{-/-}$*Ifngr*$^{-/-}$ mice.

R. parkeri Sca2 is required for disseminating from the skin to spleens and livers.

We initially hypothesized that *R. parkeri* Sca2 plays a similar pathogenic role *in vivo* to the actin-based motility factor ActA of *L. monocytogenes*, which we found is required for bacterial survival in spleens and livers upon i.v. delivery (**Fig. 3h**), in agreement with previous experiments[24,25]. However, when we examined bacterial burdens upon i.v. infection of *Ifnar*$^{-/-}$*Ifngr*$^{-/-}$ mice with *R. parkeri*, similar amounts of WT and *sca2*::Tn bacteria were recovered in spleens (**Fig. 3i**). We were also surprised to find that significantly more *sca2*::Tn than WT *R. parkeri* were recovered in livers (**Fig. 3i**). The explanation for higher *sca2*::Tn burdens in livers remains unclear. Nevertheless, these data reveal that Sca2 is likely not essential for *R. parkeri* survival in blood, invasion of host cells, or intracellular survival in spleens and livers.

We next evaluated the role for Sca2 in *R. parkeri* dissemination by measuring p.f.u. in spleens and livers following i.d. infection of *Ifnar*$^{-/-}$*Ifngr*$^{-/-}$ mice. After i.d. infection, *sca2*::Tn mutant bacteria were ~20-fold reduced in their abundance in spleens and ~2-fold reduced in their abundance in livers as compared to WT *R. parkeri* (**Fig. 3j**). Similar results were seen upon i.d. infection with lower doses of *sca2*::Tn and WT bacteria (**Fig. 3k**). Together, these results suggest that Sca2 is required for *R. parkeri* dissemination from the skin to peripheral tissue.

R. parkeri actin-based motility does not contribute to avoiding innate immunity *in vitro*.

Sca2-mediated actin-based motility is required for efficient plaque formation and cell-to-cell spread by *R. parkeri in vitro*[10,29]. However, it remains unclear if Sca2 enables *R. parkeri* to escape detection or restriction by innate immunity. The actin-based motility factor ActA enables *L. monocytogenes* to avoid autophagy[22,23], and the antimicrobial guanylate binding proteins (GBPs) inhibit *Shigella flexneri* actin-based motility[35]. We therefore sought to evaluate whether Sca2-mediated actin-based motility enables *R. parkeri* to evade innate immunity *in vitro*. We found that the *sca2*::Tn mutant grew similarly to WT bacteria in endothelial cells (**Extended Data Fig. 5a**), consistent with previous reports in epithelial cells[10,29]. We also examined whether Sca2 contributed to *R. parkeri* survival or growth in bone marrow-derived macrophages (BMDMs), which can restrict other *R. parkeri* mutants that grow normally in endothelial cells[31]. However, no significant difference in bacterial survival was observed between WT and *sca2*::Tn bacteria in BMDMs in the presence or absence of IFN-β (**Extended Data Fig. 5b**). WT and *sca2* mutant *R. parkeri* also elicited similar amounts of host cell death (**Extended Data Fig. 5c**) and IFN-I production (**Extended Data Fig. 5d**). Moreover, we found that the anti-rickettsial factor GBP2 localized to the surface of *sca2*::Tn mutant *R. parkeri* at similar frequency as with WT bacteria in the presence or absence of IFN-β (**Extended Data Fig. 5e,f**). Together, these data suggest that Sca2 does not significantly enhance the ability of *R. parkeri* to evade innate immunity *in vitro*.

Immunization with *sca2* and *ompB* mutant *R. parkeri* protects *Ifnar*$^{-/-}$*Ifngr*$^{-/-}$ mice against subsequent rechallenge.

We next examined whether *sca2*::Tn mutant *R. parkeri* elicited immunity to subsequent re-challenge with a lethal dose of WT bacteria in *Ifnar*$^{-/-}$*Ifngr*$^{-/-}$ mice. *Ifnar*$^{-/-}$*Ifngr*$^{-/-}$ mice were immunized i.v. with 5 x 10^6 *sca2*::Tn *R. parkeri* and 40 d later were intravenously re-challenged with 10^7 WT *R. parkeri*, which is approximately 10-times a 50% lethal dose (LD_{50})[33]. All mice immunized with *sca2*::Tn *R. parkeri* survived, whereas all naïve mice succumbed by 6 d.p.i. (**Fig. 6a**). We also carried out a similar test with an *R. parkeri* mutant lacking outer membrane protein B (OmpB), which is severely attenuated *in vivo*[31,33]. We intravenously infected *Ifnar*$^{-/-}$*Ifngr*$^{-/-}$ mice with 10^7 *ompB* mutant *R. parkeri* and rechallenged them 40 d later with 10^7 WT *R. parkeri*. Mice immunized with *ompB* mutant *R. parkeri* were fully

protected from the challenge, whereas naïve mice succumbed by 6 d.p.i. (**Fig. 6a**). Mice immunized with *ompB* and *sca2* mutants also did not lose weight or body temperature upon rechallenge (**Fig. 6b,c**). These data indicate that attenuated *R. parkeri* mutants elicit a robust protective immune response, and that *Ifnar*$^{-/-}$*Ifngr*$^{-/-}$ mice may serve as tools to develop live attenuated *R. parkeri* vaccine candidates.

Discussion

In this study, we show that *R. parkeri* infection of *Ifnar*$^{-/-}$*Ifngr*$^{-/-}$ mice via the i.d. route causes eschar formation, a key feature of human disease, and results in dissemination to various organs and in lethality. Using this model, we uncover a role for the *R. parkeri* actin-based motility factor Sca2 in dissemination and in causing lethal disease. We further demonstrate that attenuated *R. parkeri* mutants elicit long-lived immunity. *R. parkeri* is an emerging model to study pathogenesis of obligate cytosolic bacterial pathogens, and the animal model described here will facilitate future investigations into *R. parkeri* virulence factors, the host response to infection, the molecular determinants of human disease, and propagation of tick-borne pathogens in wildlife reservoirs.

Our study highlights the utility of mouse models that mimic natural routes of infection. Infection via the i.v. and intraperitoneal (i.p.) routes can mimic systemic disease, yet these are unnatural routes for many microbes, including food-borne, arthropod-borne, or aerosol-borne pathogens. Our observation that i.d. infection can cause lethal disease with as few as 10 bacteria (~10,000 fewer bacteria than i.v. infection[33]) suggests that *R. parkeri* may be highly adapted to reside in the skin. Infection of *Ifnar*$^{-/-}$*Ifngr*$^{-/-}$ mice via the i.d. route results in lesion formation similar to human eschars, the hallmark of *R. parkeri* infection, indicating that these mice can serve as models to better understand human disease. *Orientia tsutsugamushi* is the causative agent of scrub typhus[36], a prevalent but poorly understood tropical disease endemic to Southeast Asia[1,37,38]. *O. tsutsugamushi* also causes eschar formation in humans; however, inbred mice do not recapitulate eschar formation during *O. tsutsugamushi* infection[5], similar to *R. parkeri* infection. The *Ifnar*$^{-/-}$*Ifngr*$^{-/-}$ model might therefore serve as a tool to investigate the pathogenesis of other arthropod-borne pathogens, including *O. tsutsugamushi*. Lastly, saliva from ticks, mosquitos, and sand flies enhances pathogenesis of arthropod-

borne bacterial, viral, and parasitic pathogens[39–41], and non-human primates inoculated with *R. parkeri* exhibited altered inflammatory responses when administered after tick-bite[42]. This may suggest a potential role for tick vector components such as tick saliva in *R. parkeri* pathogenesis. Developing improved murine infection models that mimic the natural route of infection, including with the tick vector, is critical to better understand the virulence and transmission of tick-borne pathogens.

Many *Rickettsia* species, as well as many facultative cytosolic pathogens including *L. monocytogenes*, undergo actin-based motility to spread from cell to cell. For *L. monocytogenes*, the actin-based motility factor ActA enables the pathogen to survive *in vivo*, as *actA* mutant bacteria are over 1,000-fold attenuated by measuring lethality[26,27] and by enumerating bacteria in spleens and livers of mice after i.v. infection[24,25]. However, the pathogenic role for actin-based motility in the Rickettsiae has remained unclear. We find that Sca2 is not required for intracellular survival in organs upon i.v. infection of *Ifnar*$^{-/-}$*Ifngr*$^{-/-}$ mice, but rather, is required for dissemination from skin to peripheral organs and lethality upon i.d. infection. Consistent with an important role for Sca2 in pathogenesis, a previous study reported that i.v. infection of guinea pigs with *sca2* mutant *R. rickettsii* did not elicit fever[29]. Our results suggest that Sca2-mediated actin-based motility by *Rickettsia* may facilitate dissemination through host reservoirs, although we cannot rule out other roles for Sca2 that do not involve actin assembly. *R. prowazekii* and *R. typhi*, which cause severe human disease, encode a fragmented *sca2* gene[43], and undergo no or dramatically reduced frequency of actin-based motility, respectively[44,45]. Although it remains unclear why some *Rickettsia* species lost the ability to undergo actin-based motility, Sca2 is dispensable for *R. parkeri* dissemination in the tick vector[32], suggesting that actin-based motility may play a specific role in dissemination within mammalian hosts.

We find that *sca2* mutant *R. parkeri*, as well as *ompB* mutant *R. parkeri*, elicit a robust protective immune response in *Ifnar*$^{-/-}$*Ifngr*$^{-/-}$ mice. These findings complement previous observations that *sca2* mutant *R. rickettsii* elicits antibody responses in guinea pigs[29], and expands upon these findings by demonstrating protection from rechallenge and revealing additional vaccine candidates. There are currently limited vaccine candidates that protect against rickettsial disease[6]. Identifying new vaccine candidates may reveal avenues to protect against tick-borne infections and aerosolized *Rickettsia*,

which are extremely virulent and potential bioterrorism agents[46], as well as against Brill-Zinsser disease, caused by latent *R. prowazekii*[6]. Future studies exploring whether attenuated *R. parkeri* mutants provide immunity against other *Rickettsia* species are warranted to better define the mechanisms of protection. Finally, we note that these findings on immunity may help develop *R. parkeri* as an antigen delivery platform. *R. parkeri* resides directly in the host cytosol for days and could potentially be engineered to secrete foreign antigens for presentation by major histocompatibility complex I. In summary, the mouse model described here will facilitate future investigations into numerous aspects of *R. parkeri* infection, including actin-based motility and immunity, and may serve as model for other arthropod-borne pathogens.

Figures

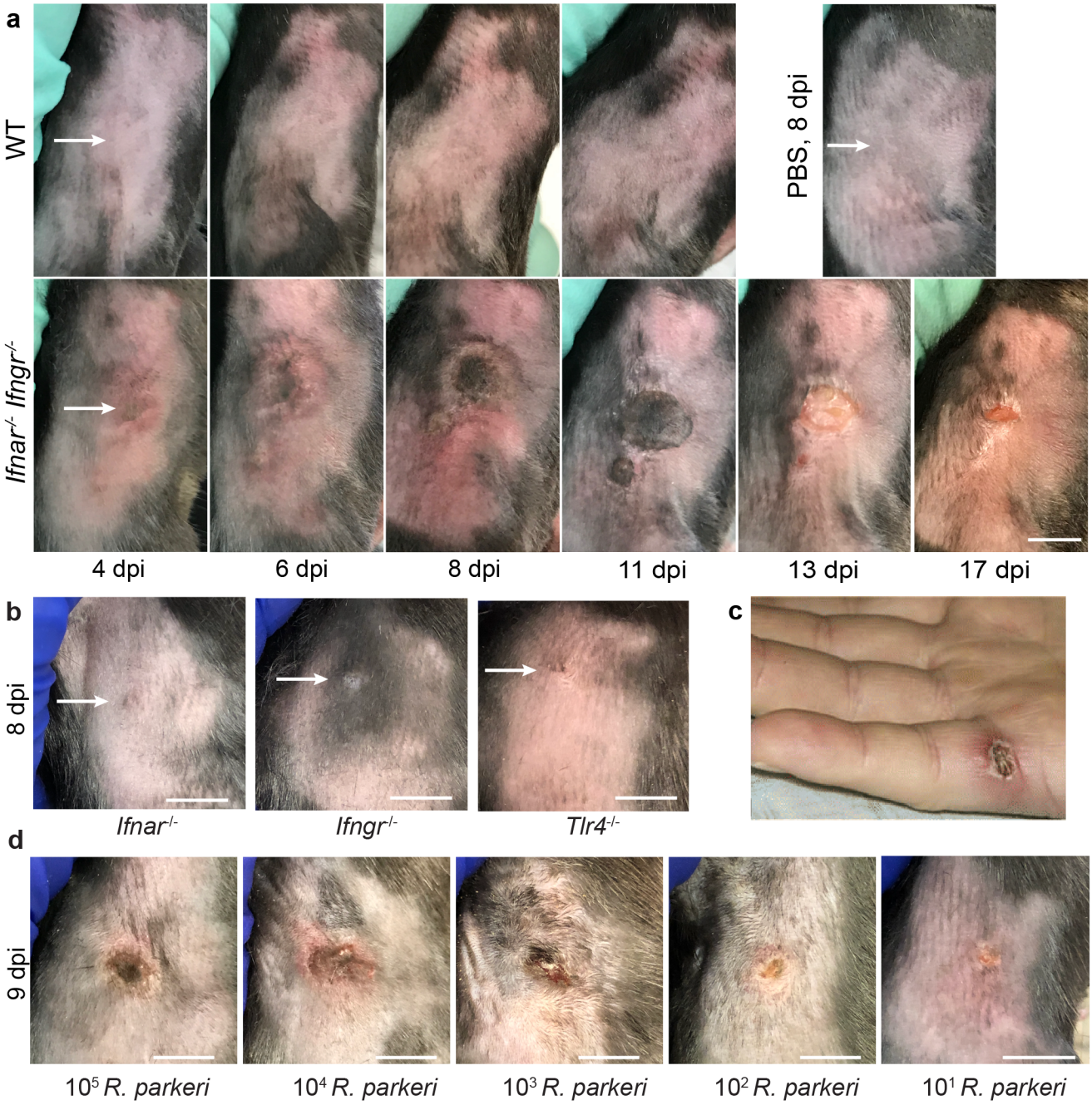

Fig. 1: **I.d. infection of *Ifnar*$^{-/-}$*Ifngr*$^{-/-}$ mice with *R. parkeri* elicits skin lesions that are grossly similar to human eschars.**

a) Representative images of WT and *Ifnar*$^{-/-}$*Ifngr*$^{-/-}$ mice after i.d. inoculation with 10^7 *R. parkeri* (or PBS, in top right image only). Data are representative of 3 independent experiments. White arrows indicate the injection site on the right flank of the mouse. Scale bar, 1 cm. **b**) Representative images of *Ifnar*$^{-/-}$, *Ifngr*$^{-/-}$, and *Tlr4*$^{-/-}$ mice, infected intradermally with 10^7 WT *R. parkeri.* White arrows indicate the infection site on the right flank of the mouse. Scale bar, 1 cm. Data are representative of three independent experiments. **c**) Gross pathology of a human *R. parkeri* infection, from Paddock *et al*[7]. **d**) Representative images of *Ifnar*$^{-/-}$*Ifngr*$^{-/-}$ mice infected intradermally with the indicated amounts of WT *R. parkeri* at 9 d.p.i. Scale bar, 1 cm. Data are representative from two independent experiments.

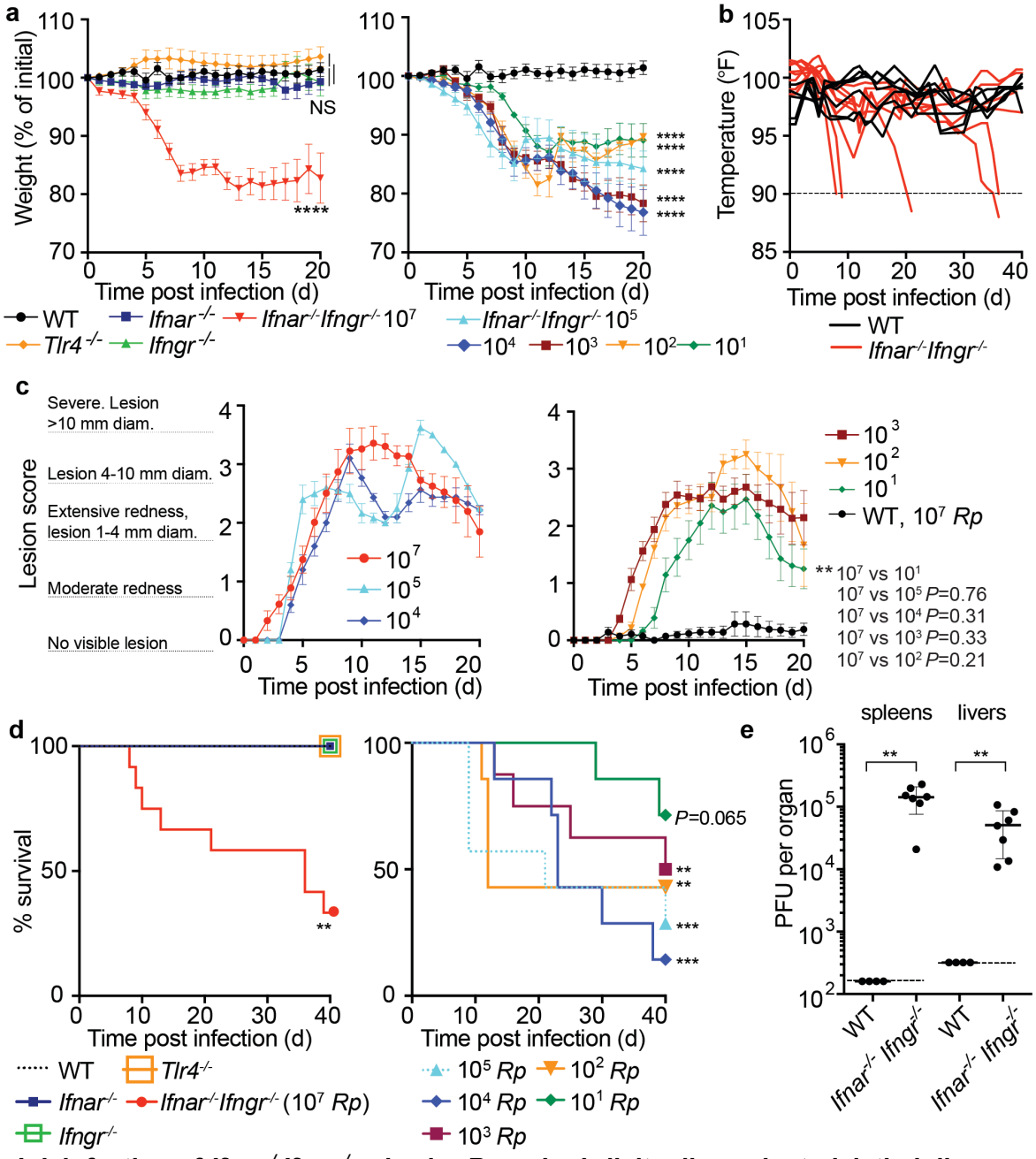

Fig. 2: I.d. infection of *Ifnar*$^{-/-}$*Ifngr*$^{-/-}$ mice by *R. parkeri* elicits disseminated, lethal disease.

a) Weight changes over time in mice infected i.d. with *R. parkeri*. Data are shown as a percentage change to initial weight. In the left panel, all mice were infected with 10^7 *R. parkeri*; *n*=7 (WT), *n*=10 (*Ifnar*$^{-/-}$), *n*=7 (*Ifngr*$^{-/-}$), *n*=9 (*Ifnar*$^{-/-}$*Ifngr*$^{-/-}$) and 4 (*Tlr4*$^{-/-}$) individual mice. In the right panel, *Ifnar*$^{-/-}$*Ifngr*$^{-/-}$ mice were infected with the indicated amounts of *R. parkeri*; *n*=7 (10^5 *R. parkeri*), *n*=7 (10^4 *R. parkeri*), *n*=8 (10^3 *R. parkeri*), *n*=7 (10^2 *R. parkeri*), *n*=7 (10^1 *R. parkeri*) individual mice. WT data is the same in both panels. Data for each genotype are combined from two or three independent experiments. **b**) Temperature changes over time in mice intradermally infected with 10^7 *R. parkeri.* Each line is an individual mouse. Mice were euthanized if their temperature fell below 90° F, as indicated by the dotted line. Data are the combination of three independent experiments with *n*=7 (WT) and 9 (*Ifnar*$^{-/-}$*Ifngr*$^{-/-}$) individual mice. **c**) Analysis of gross skin pathology after i.d. infection. *Ifnar*$^{-/-}$*Ifngr*$^{-/-}$ mice were infected with the indicated number of *R. parkeri* and monitored over time. WT mice were infected with 10^7 *R. parkeri*. Data are the combination of three independent experiments for WT and the 10^7 dose in *Ifnar*$^{-/-}$*Ifngr*$^{-/-}$ mice; data for all other doses are the combination of two independent experiments. *n*=9 (10^7), *n*=5 (10^5), *n*=5 (10^4), *n*=8 (10^3), *n*=7 (10^2), *n*=7 (10^1), and *n*=7 (WT) individual mice. **d**) Mouse survival after i.d. infection with *R. parkeri.* In the left panel, all mice were infected with 10^7 *R. parkeri*; *n*=7 (WT), *n*=11 (*Ifnar*$^{-/-}$), *n*=8 (*Ifngr*$^{-/-}$), *n*=4 *Tlr4*$^{-/-}$, and *n*=12 (*Ifnar*$^{-/-}$*Ifngr*$^{-/-}$) individual mice. Data are the combination of three separate experiments for WT, *Ifnar,* and *Ifnar*$^{-/-}$*Ifngr*$^{-/-}$ and two separate experiments for *Ifngr*$^{-/-}$ and *Tlr4*$^{-/-}$. In the right panel, *Ifnar*$^{-/-}$*Ifngr*$^{-/-}$ mice were infected with the indicated amounts of *R. parkeri.* Data are the combination of two independent experiments; *n*=7 (10^5), *n*=7 (10^4), *n*=8 (10^3), *n*=7 (10^2), and *n*=7 (10^1) individual mice. **e**) Bacterial burdens in organs of intradermally infected WT and *Ifnar*$^{-/-}$*Ifngr*$^{-/-}$ mice. Mice were intradermally inoculated with 10^7 *R. parkeri*, and spleens and livers were harvested and plated for p.f.u. at 72 h.p.i. Dotted lines indicate the limit of detection. Data are the combination of two independent experiments. *n*=4 (WT) and 7 (*Ifnar*$^{-/-}$*Ifngr*$^{-/-}$) individual mice. Data in **a**, **c** are the mean ± SEM. Statistical analyses in **a** used a two-way ANOVA where each group was compared to WT at t=20 d.p.i. Statistical analyses in **c** used a two-way ANOVA at t=20 d.p.i. Statistical analyses in **d** used a log-rank (Mantel-Cox) test to compare *Ifnar*$^{-/-}$ to *Ifnar*$^{-/-}$*Ifngr*$^{-/-}$ at each dose. Statistical analysis in **e** used a two-tailed Mann-Whitney U test. NS, not significant; ***P*<0.01; ****P*<0.001; *****P*<0.0001.

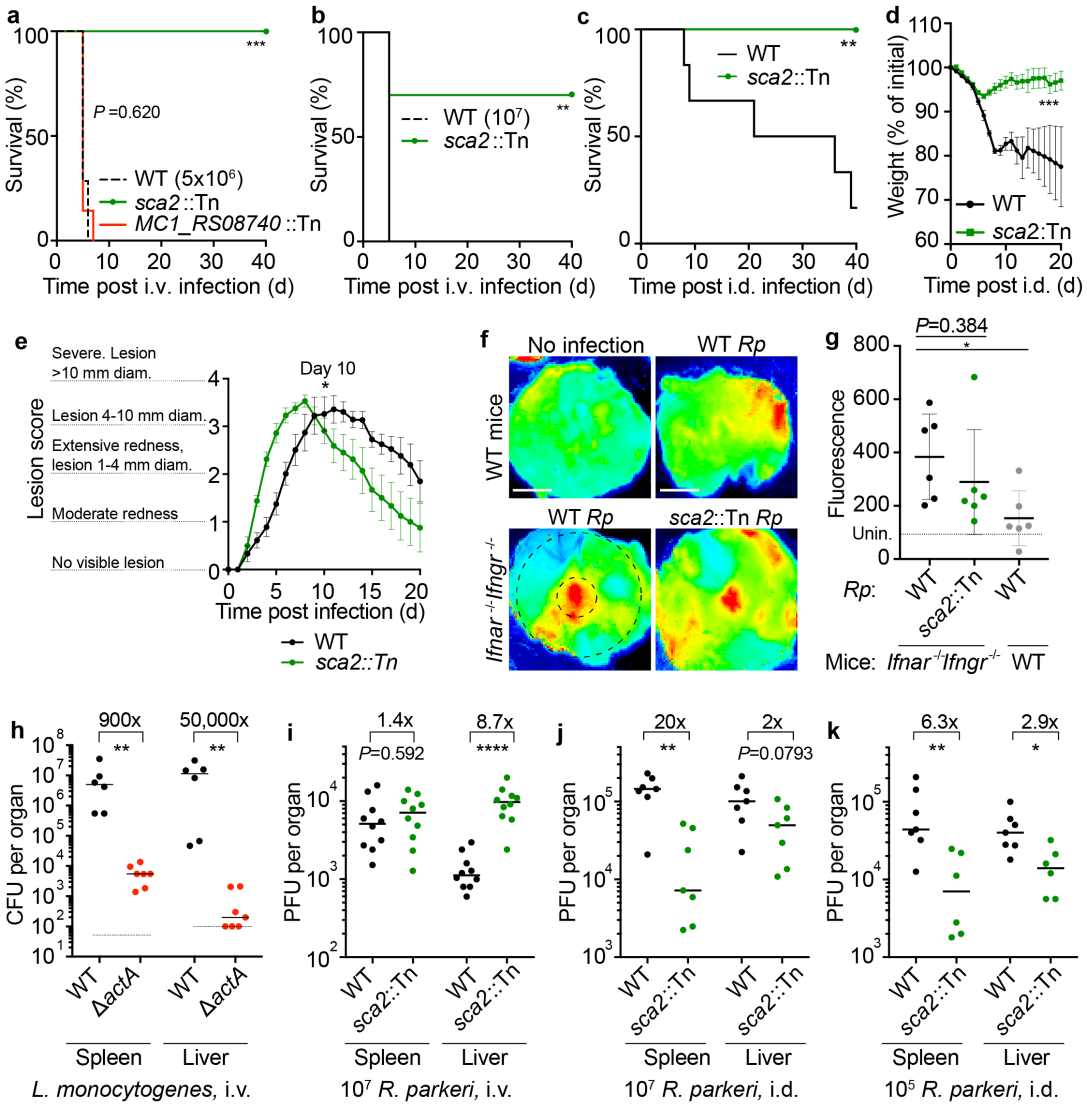

Figure 3: *R. parkeri* Sca2 contributes to dissemination from skin to peripheral organs.

a) Survival of *Ifnar*$^{-/-}$*Ifngr*$^{-/-}$ mice upon i.v. infection with 5 x 10^6 *R. parkeri*. *n*=7 (WT), 10 (*sca2*::Tn), and 7 (*MC1_RS08740*::Tn *R. parkeri*) individual mice. Data are the combination of two independent experiments.**b**) Survival of *Ifnar*$^{-/-}$*Ifngr*$^{-/-}$ mice upon i.v. infection with 10^7 *R. parkeri*. *n*=7 (WT) and 10 (*sca2*::Tn) individual mice. Data are the combination of two independent experiments. **c**) Survival of *Ifnar*$^{-/-}$*Ifngr*$^{-/-}$ mice upon i.d. infection with 10^7 *R. parkeri*. *n*=6 (WT) and 8 (*sca2*::Tn) individual mice. Data are the combination of two independent experiments. **d**) Weight changes of *Ifnar*$^{-/-}$*Ifngr*$^{-/-}$ mice upon i.d. infection with 10^7 *R. parkeri*. *n*=6 (WT) and 8 (*sca2*::Tn) individual mice. Data are the combination of two independent experiments. **e**) Analysis of gross skin pathology after i.d. infection. *Ifnar*$^{-/-}$*Ifngr*$^{-/-}$ mice were infected with 10^7 of the indicated strains of *R. parkeri* and monitored over time. *n*=9 (WT) and 8 (*sca2*::Tn) individual mice. Data are the combination of two independent experiments. **f**) Representative images of fluorescence in mouse skin after i.d. infection with 10^6 *R. parkeri* and delivery of a fluorescent dextran, at 5 d.p.i. Scale bars, 1 cm. The larger black dashed circle represents the area that was measured for fluorescence for each sample, as indicated in **Fig. 3g** (~80,000 pixels). The smaller black-dashed circle represents of the injection site area that was measured for fluorescence for each sample, as indicated in **Extended Data Fig. 3** (~7,800 pixels). **g**) Quantification of fluorescence in mouse skin after i.d. infection. Mice were infected with 10^7 *R. parkeri*, and 150 µl fluorescent dextran was intravenously delivered at 5 d.p.i. Skin was harvested 2 h later, and fluorescence was measured using a fluorescence imager. Data indicate measurements of larger areas of skin, as indicated in **f** by the larger black circle. *n*=6 (WT *R. parkeri*) and *n*=6 (*sca2*::Tn *R. parkeri*) individual *Ifnar*$^{-/-}$*Ifngr*$^{-/-}$ mice; *n*=6 (WT *R. parkeri*) individual WT mice. For each experiment, the average of uninfected samples was normalized to 100; each sample was divided by the average for uninfected mice and multiplied by 100; the dotted horizontal line indicates 100 arbitrary units, corresponding to uninfected (unin.) mice. Data are the combination of two independent experiments. **h**) Quantification of *L. monocytogenes* abundance in organs of WT C57BL/6J mice upon i.v. infection with 10^4 bacteria, at 72 h.p.i. Data are the combination of two independent experiments. n=6 (WT), n=7 (Δ*actA*) individual mice. **i**) Quantification of *R. parkeri* abundance in spleens and livers of WT C57BL/6J mice upon i.v. infection, at 72 h.p.i. Data are the combination of two independent experiments. *n*=10 (WT) and 10 (*Sca2*::Tn) individual mice. **j**) Quantification of *R. parkeri* abundance in organs upon i.d. infection with 10^7 *R. parkeri*. *n*=7 (WT) and 7 (*sca2*::Tn) individual mice. Data are the combination of two independent experiments. Data for WT *R. parkeri* in *Ifnar*$^{-/-}$*Ifngr*$^{-/-}$ mice are the same as in **Fig. 2e**. **k**) Quantification of *R. parkeri* abundance in organs upon i.d. infection with 10^5 *R. parkeri*. *n*=7 (WT) and 6 (*sca2*::Tn). Data are the combination of two independent experiments. Solid horizontal bars in **g** indicate means; solid horizontal bars in **h**-**k** indicate medians; error bars indicate SD. Statistical analyses for survival in **a, b, c** used a log-rank (Mantel-Cox) test. Statistical analysis in **d** used a two-way ANOVA at t=20. Statistical analysis in **e** used a two-way ANOVA from 0 to 10 d.p.i. Statistical analyses in **g** used a two-tailed Student's T test. Statistical analyses in **h, i, j, k** used a two-tailed Mann-Whitney U test. The fold change in **h, i, j, k** indicates differences of medians. **P*<0.05; ***P*<0.01; ****P*<0.001; *****P*<0.0001.

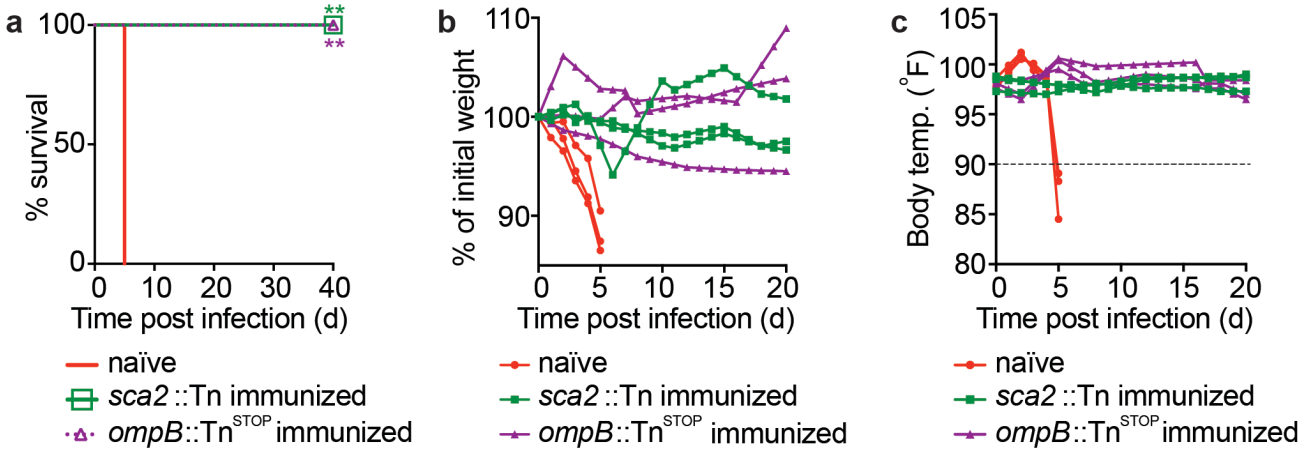

Figure 4: *ompB* and *sca2* mutant *R. parkeri* elicit immunity in *Ifnar*$^{-/-}$*Ifngr*$^{-/-}$ mice.

a) Survival of immunized and naïve *Ifnar*$^{-/-}$*Ifngr*$^{-/-}$ mice upon i.v. *R. parkeri* infection. Immunized mice were first infected with 5x10^6 *sca2*::Tn or 10^7 *ompB*:Tn^{STOP} *R. parkeri* and were re-challenged 40 d later with 10^7 WT *R. parkeri*. *n*=6 (naïve); *n*=5 (*sca2*::Tn immunized); *n*=5 (*ompB*::Tn^{STOP} immunized) individual mice. Data are the combination of two independent experiments.

b) Weight changes over time in mice infected i.d. with 10^7 *R. parkeri*. Data are representative of two independent experiments. *n*=3 (naïve); *n*=3 (*sca2*::Tn immunized); *n*=3 (*ompB*::Tn^{stop} immunized) individual mice. Each line represents an individual mouse.

c) Temperature changes over time in mice infected i.d. with 10^7 *R. parkeri.* Data are representative from two independent experiments. *n*=3 (naïve); *n*=3 (*sca2*::Tn immunized); *n*=3 (*ompB*::Tn^{STOP} immunized) individual mice. Each line represents an individual mouse. Statistical analyses in **a** used a log-rank (Mantel-Cox) test to compare each group of immunized mice to naïve mice. ***P*<0.01.

Extended Data Figures

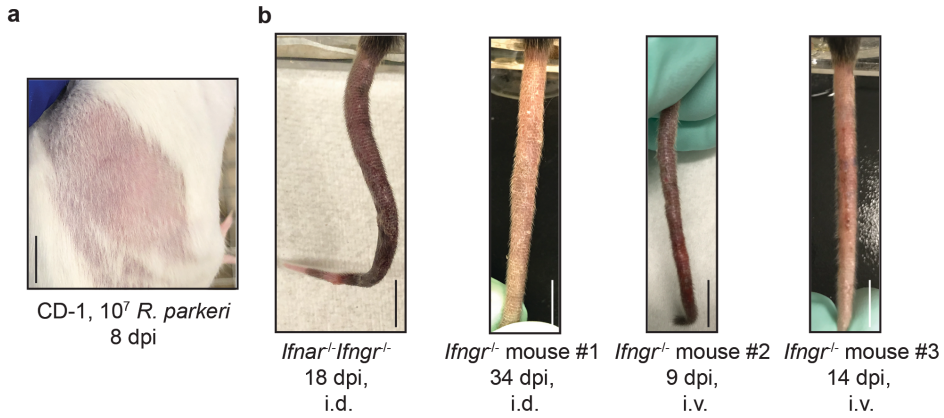

Extended Data Fig. 1: *Ifnar*$^{-/-}$*Ifngr*$^{-/-}$ mice develop disseminated disease upon intradermal *R. parkeri* infection.

a) Representative image of the right flank of CD-1 mice intradermally infected with 10^7 *R. parkeri*. Scale bar, 1 cm. Data are representative from two independent experiments.

b) Representative images of tails of *Ifnar*$^{-/-}$*Ifngr*$^{-/-}$ and *Ifngr*$^{-/-}$ mice, infected via the i.v. or i.d. route (as indicated), with 10^7 WT *R. parkeri.* Some *Ifnar*$^{-/-}$*Ifngr*$^{-/-}$ and *Ifngr*$^{-/-}$ mice had no gross pathological symptoms in the tail, whereas some mice exhibited inflamed, necrotic tails at various times post infection. Scale bar, 1 cm. Data are representative from three independent experiments.

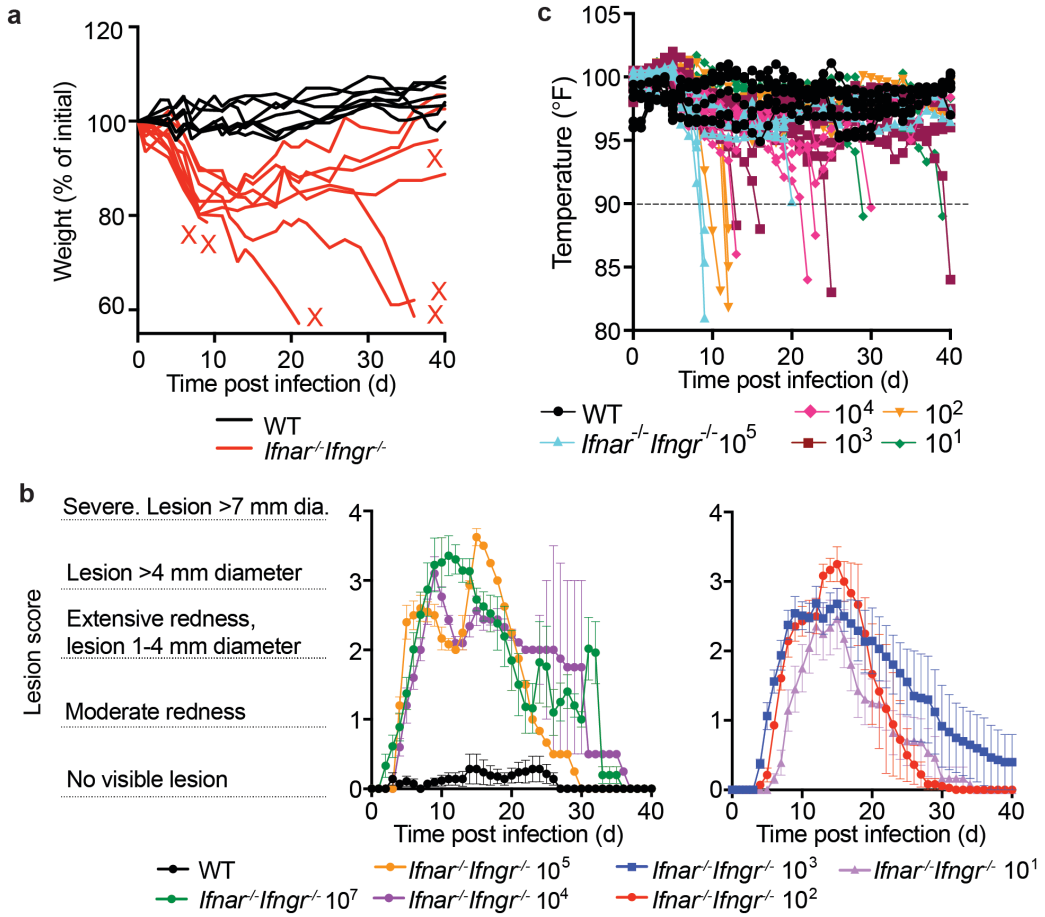

Extended Data Fig. 2: *Ifnar*$^{-/-}$ or *Ifngr*$^{-/-}$ mice develop limited disease upon intradermal infection, and *Ifnar*$^{-/-}$*Ifngr*$^{-/-}$ develop lesions of dose-dependent severity.

a) Weight changes over time in mice intradermally infected with 10^7 WT *R. parkeri*. Data are the combination of two independent experiments for WT and three for *Ifnar*$^{-/-}$*Ifngr*$^{-/-}$; *n*=7 (WT) and *n*=9 (*Ifnar*$^{-/-}$*Ifngr*$^{-/-}$) individual mice. Each line is an individual mouse.

b) Gross pathological analysis of the skin infection site after i.d. infection. *Ifnar*$^{-/-}$*Ifngr*$^{-/-}$ mice were infected with the indicated number of *R. parkeri* and monitored over time. Data are the combination of three independent experiments for the 10^7 dose and two independent experiments for all other doses. *n*=7 (WT), *n*=9 (10^7), *n*=5 (10^5), *n*=5 (10^4), *n*=8 (10^3), *n*=7 (10^2), and *n*=7 (10^1) individual mice. Data are the same as in **Fig. 2c** but are extended to 40 d.p.i.

c) Temperature changes over time in mice infected i.d. with the indicated amounts of WT *R. parkeri.* Data are the combination of two independent experiments; *n*=7 (WT), *n*=7 (10^5), *n*=7 (10^4), *n*=8 (10^3), *n*=7 (10^2), and *n*=7 (10^1) individual mice. Each bar represents an individual mouse. Mice were euthanized if their body temperature fell below 90° F, as indicated by the dotted line.

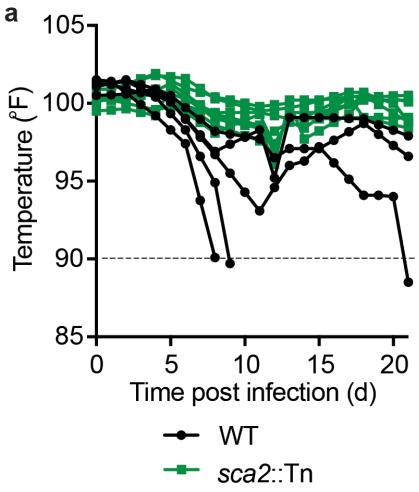

Extended Data Fig. 3: Intradermal infection of *Ifnar*$^{-/-}$*Ifngr*$^{-/-}$ mice with *sca2*::Tn *R. parkeri* causes less severe temperature loss as compared to WT bacteria.

a) Temperature changes over time in mice infected i.d. with 10^7 *R. parkeri.* Data are the combination of two independent experiments; *n*=5 (WT), *n*=8 (*sca2*::Tn) individual mice. Each line represents an individual mouse. Mice were euthanized if their body temperature fell below 90° F, as indicated by the dotted line.

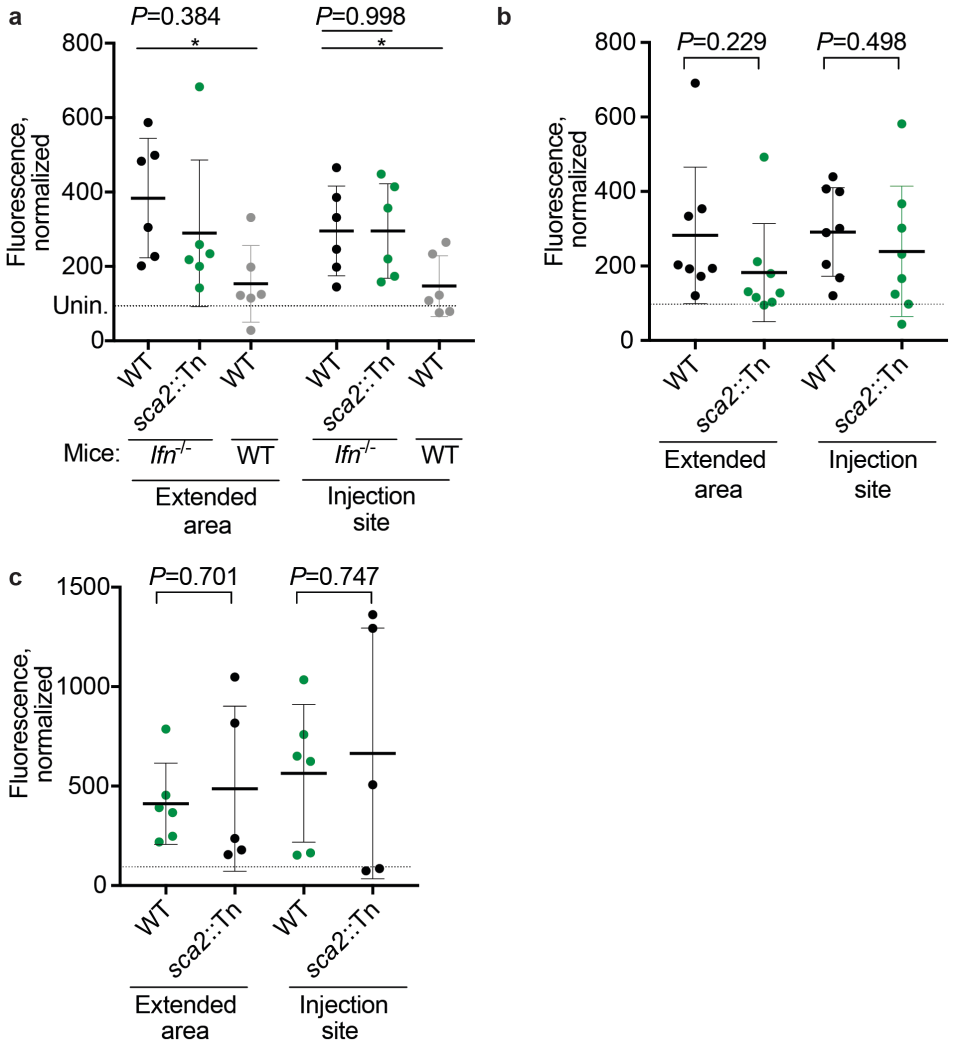

Extended Data Fig. 4: WT and *sca2*::Tn *R. parkeri* elicit similar amounts of vascular damage in skin upon i.d. infection of *Ifnar*$^{-/-}$*Ifngr*$^{-/-}$ mice.

a) Quantification of fluorescence in mouse skin after i.d. infection. Mice were infected i.d. with 10^7 *R. parkeri* and fluorescent dextran was intravenously delivered at 5 d.p.i. Skin was harvested 2 h after delivery of dextran and analyzed with a fluorescence imager. *n*=6 (WT *R. parkeri*) and *n*=6 (*sca2*::Tn *R. parkeri*) individual *Ifnar*$^{-/-}$*Ifngr*$^{-/-}$ mice; *n*=6 (WT *R. parkeri*) individual WT mice. Data in the 'extended area' are the same as those reported in **Fig. 3e**. **b**) Quantification of fluorescence in mouse skin after i.d. infection. Mice were infected i.d. with 10^6 *R. parkeri*, and fluorescent dextran was intravenously delivered at 5 d.p.i. Skin was harvested 2 h after delivery of dextran and analyzed with a fluorescence imager. *n*=8 (WT *R. parkeri*) and *n*=8 (*sca2*::Tn *R. parkeri*) individual *Ifnar*$^{-/-}$*Ifngr*$^{-/-}$ mice. **c**) Quantification of fluorescence in mouse skin after i.d. infection. Mice were infected i.d. with 10^5 *R. parkeri* and fluorescent dextran was intravenously delivered at 5 d.p.i. Skin was harvested 2 h after delivery of dextran and analyzed with a fluorescence imager. *n*=6 (WT *R. parkeri*) and *n*=5 (*sca2*::Tn *R. parkeri*) individual *Ifnar*$^{-/-}$*Ifngr*$^{-/-}$ mice. For each experiment, the average of uninfected samples was normalized to 100, and each sample was divided by the average for uninfected mice and multiplied by 100; the dotted horizontal line indicates 100 arbitrary units, corresponding to uninfected (unin.) mice. Representative sizes for the larger 'extended areas' of skin and the smaller 'injection site' areas of skin are indicated in **Fig. 3d**. Data in **a-c** are each the combination of two independent experiments. Solid horizontal bars indicate means; error bars indicate SD. For statistical analyses, a two-tailed Student's T test was used to compare the indicated samples.

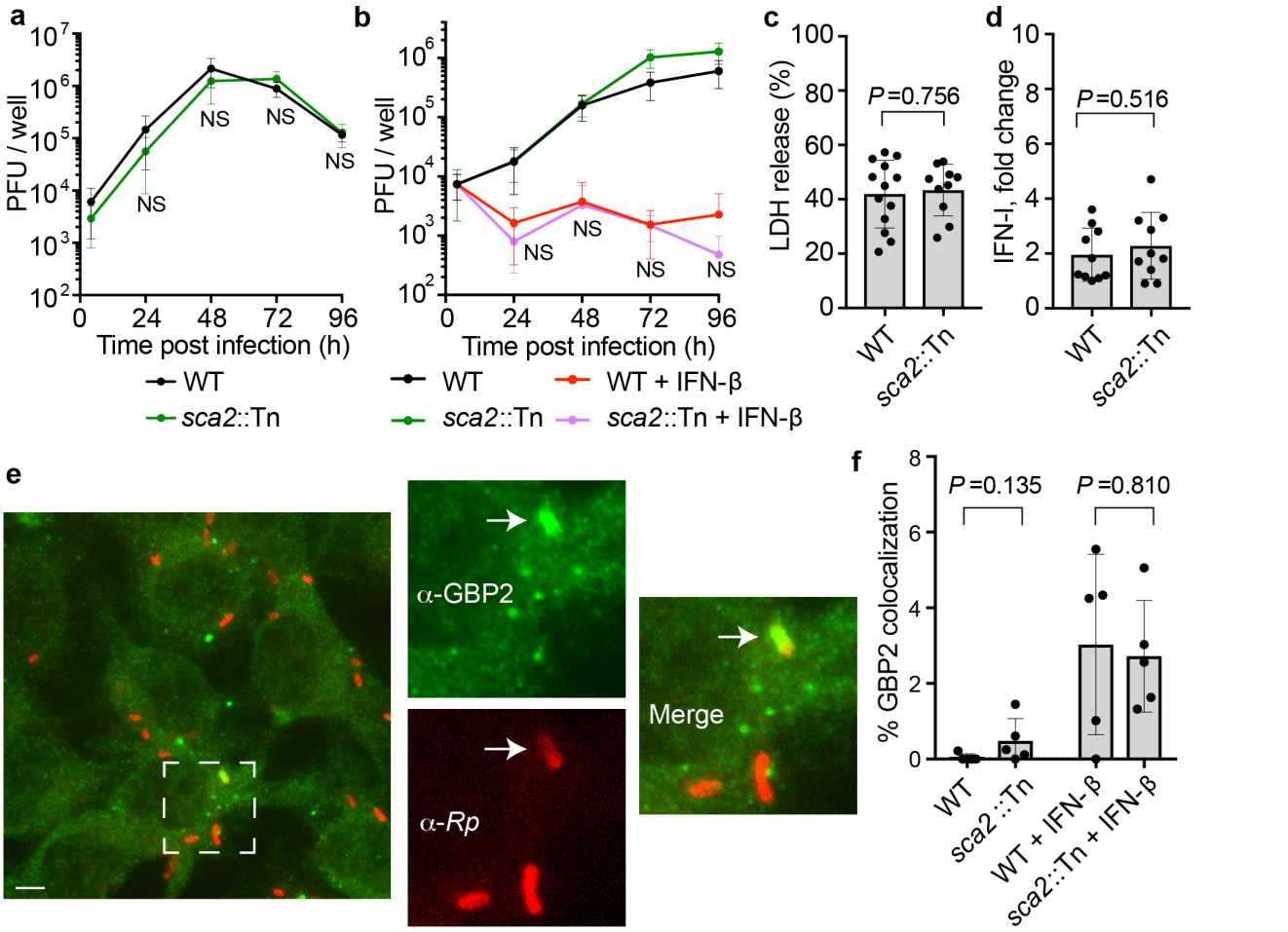

Extended Data Fig. 5: Sca2 does not significantly enhance *R. parkeri* avoidance of antibacterial innate immune responses *in vitro*.

a) *R. parkeri* abundance in HMEC-1s, multiplicity of infection (MOI) of 0.2. Data are the combination of three independent experiments, each with two biological replicates. For statistics, a two-tailed Student's T test was used to compare WT to *sca2*::Tn at 48, 72, and 96 h.p.i. No statistically significant differences were observed at any time. **b**) *R. parkeri* abundance in BMDMs, MOI of 1. Data are the combination of three independent experiments, each with two biological replicates. Data were normalized by multiplying fold difference between WT and *Sca2*::Tn at 4 h.p.i. to *Sca2*::Tn and *Sca2*::Tn + IFN-I data at all time points.**c**) Host cell death upon *R. parkeri* infection of BMDMs, as measured by lactate dehydrogenase (LDH) release assay, MOI of 1. From left to right, *n*=6 and 3 biological replicates and are the combination of two independent experiments. **d**) IFN-I abundance in supernatants of infected BMDMs (24 h.p.i.; MOI of 1), measured using a luciferase reporter assay. The data show the fold change over uninfected cells. *n*=7 and 7 biological replicates and are the combination of two independent experiments. **e**) A representative image using x100 confocal immunofluorescence microscopy of WT BMDMs infected with *sca2*::Tn *R. parkeri* in the presence of 100 U recombinant IFN-β (3 h.p.i.; MOI of 1). Green, α-GBP2; red, α-*Rickettsia* (*Rp*). The dotted square indicates the image that is expanded in the other images, separated into two individual and one merged channel. Scale bars, 2.5 μm. White arrows indicate a bacterium that colocalizes with GBP2. Data are representative of three independent experiments. **f**) Quantification of GBP2 colocalization with *R. parkeri* in BMDMs at 24 h.p.i. Each data point is an average of at least five separate images totaling >150 bacteria. Data are the combination of three independent experiments. Statistical analyses used a two-tailed Student's T test. NS, not significant. Data in **a**,**b** are means; bars in **c**, **d**, and **f** are means; error bars indicate SD.

Methods

Bacterial preparations

R. parkeri strain Portsmouth was originally obtained from Dr. Christopher Paddock (Centers for Disease Control and Prevention). To amplify *R. parkeri*, confluent monolayers of female African green monkey kidney epithelial Vero cells (obtained from UC Berkeley Cell Culture Facility, tested for mycoplasma contamination, and authenticated by mass spectrometry) were infected with 5 x 10^6 *R. parkeri* per T175 flask. Vero cells were grown in DMEM (Gibco 11965-092) containing 4.5 gl^{-1} glucose and 2% fetal bovine serum (FBS; GemCell). Infected cells were scraped and collected at 5 or 6 d.p.i. when ~90% of cells were rounded due to infection. Scraped cells were then centrifuged at 12,000*g* for 20 min at 4˚C. Pelleted cells were resuspended in K-36 buffer (0.05 M KH_2PO_4, 0.05 M K_2HPO_4, 100 mM KCl, 15 mM NaCl, pH 7) and dounced for ~40 strokes at 4˚C. The suspension was then centrifuged at 200*g* for 5 min at 4˚C to pellet host cell debris. Supernatant containing *R. parkeri* was overlaid on a 30% MD-76R (Merry X-Ray) gradient solution in ultracentrifuge tubes (Beckman/Coulter Cat 344058). Gradients were centrifuged at 18,000 r.p.m. in an SW-28 ultracentrifuge swinging bucket rotor (Beckman/Coulter) for 20 min at 4˚C. These '30% prep' bacterial pellets were resuspended in brain heart infusion (BHI) media (BD, 237500), aliquoted, and stored at -80˚C. Titers were determined by plaque assays by serially diluting the *R. parkeri* in 6-well plates containing confluent Vero cells. Plates were spun for 5 min at 300*g* in an Eppendorf 5810R centrifuge and at 24 h post infection (h.p.i.); the media from each well was aspirated, and the wells were overlaid with 4 ml/well DMEM with 5% FBS and 0.7% agarose (Invitrogen, 16500-500). At 6 d.p.i., an overlay of 0.7% agarose in DMEM containing 2.5% neutral red (Sigma, N6264) was added. Plaques were then counted 24 h later. For infections with *ompB* mutant bacteria, the *ompB*^{STOP}::Tn mutant was used, which contains a transposon and an upstream stop codon in *ompB,* as previously described[31].

Deriving bone marrow macrophages

For obtaining bone marrow, male or female mice were euthanized, and femurs, tibias, and fibulas were excised. Bones were sterilized with 70% ethanol and washed with BMDM media (20% FBS (HyClone), 0.1% β-mercaptoethanol, 1% sodium pyruvate, 10% conditioned supernatant from 3T3 fibroblasts, in DMEM (Gibco) with 4.5 gl^{-1} glucose and 100 µg/ml streptomycin and 100 U/ml penicillin), and ground with a mortar and pestle. Bone homogenate was passed through a 70 µm nylon cell strainer (Thermo Fisher Scientific, 08-771-2) for particulate removal. Filtrates were then centrifuged at 290*g* in an Eppendorf 5810R centrifuge for 8 min, supernatant was aspirated, and the pellet was resuspended in BMDM media. Cells were plated in 30 ml BMDM media in non-TC-treated 15 cm petri dishes at a ratio of 10 dishes per 2 femurs/tibias and incubated at 37˚ C. An additional 30 ml of BMDM media was added 3 d later. At 7 d the media was aspirated, 15 ml cold PBS (Gibco, 10010-023) was added, and cells were incubated at 4˚C with for 10 min. BMDMs were scraped from the plate, collected in a 50 ml conical tube, and centrifuged at 290*g* for 5 min. PBS was aspirated, and cells were resuspended in BMDM media with 30% FBS and 10% DMSO at 10^7 cells/ml. 1 ml aliquots were stored at -80° C for 24 h in Styrofoam boxes and then moved to long-term storage in liquid nitrogen.

Infections *in vitro*

HMEC-1 cells (obtained from the UC Berkeley Cell Culture Facility and authenticated by short-tandem-repeat analysis) were passaged 2-3 times weekly and grown at 37° C with 5% CO_2 in DMEM containing 10 mM L-glutamine (Sigma, M8537), supplemented with 10% heat-inactivated FBS (HyClone), 1 µg/mL hydrocortisone (Spectrum Chemical, CO137), 10 ng/mL epidermal growth factor (Thermo Fisher Scientific, CB40001; Corning cat. no. 354001), and 1.18 mg/mL sodium bicarbonate. HMEC media was prepared every 1-2 months, and aliquoted and stored at 4°C. To prepare HMEC-1 cells for infection, cells were treated with 0.25% trypsin-EDTA (Thermo Fisher Scientific); the number of cells was counted using a hemocytometer (Bright-Line), and 3 x 10^4 cells were plated into 24-well plates 48 h prior to infection.

To plate macrophages for infection, BMDM aliquots were thawed on ice, diluted into 9 ml of DMEM, centrifuged at 290*g* for 5 min in an Eppendorf 5810R centrifuge, and the pellet was resuspended in 10 ml BMDM media without antibiotics. 5 x 10^5 cells were plated into 24-well plates. Approximately

16 h later, "30% prep" *R. parkeri* were thawed on ice and diluted into fresh BMDM media to either 10^6 p.f.u./ml or $2x10^5$ p.f.u./ml. Media was then aspirated from the BMDMs, replaced with 500 µl media containing *R. parkeri,* and plates were spun at 300*g* for 5 min in an Eppendorf 5810R centrifuge. Infected cells were incubated in a humidified CEDCO 1600 incubator set to 33˚C and 5% CO_2. Recombinant mouse IFN-β (PBL, 12405-1) was added directly to infected cells after spinfection.

For measuring p.f.u., supernatants from infected BMDMs were aspirated, and each well was washed twice with 500 µl sterile milli-Q-grade water. After adding 1 ml of sterile milli-Q water to each well, macrophages were lysed by repeated pipetting. Serial dilutions of lysates were added to confluent Vero cells in 12 well plates. Plates were spun at 300*g* using an Eppendorf 5810R centrifuge for 5 min at room temperature and incubated at 33˚C overnight. At ~16 h.p.i., media was aspirated and replaced with 2 ml/well of DMEM containing 0.7% agarose and 5% FBS (GemCell). At ~6 d.p.i., 1 ml of DMEM containing 0.7% agarose, 1% FBS (GemCell), 200 µg/ml amphotericin B (Invitrogen, 15290-018), and 2.5% neutral red (Sigma) was added to each well. Plaques were then counted after 24 h.

Microscopy, LDH, and IFN-I experiments were performed as described[33].

Animal experiments

Animal research was conducted under a protocol approved by the University of California, Berkeley Institutional Animal Care and Use Committee (IACUC) in compliance with the Animal Welfare Act and other federal statutes relating to animals and experiments using animals (Welch lab animal use protocol AUP-2016-02-8426). The University of California, Berkeley IACUC is fully accredited by the Association for the Assessment and Accreditation of Laboratory Animal Care International and adheres to the principles of the Guide for the Care and use of Laboratory Animals[47]. Mouse infections were performed in a biosafety level 2 facility. All animals were maintained at the University of California, Berkeley campus, and all infections were performed in accordance with the approved protocols. Mice were between 8 and 20 weeks old at the time of initial infection. Mice were selected for experiments based on their availability, regardless of sex. A statistical analysis was not performed to predetermine sample size prior to initial experiments. Initial sample sizes were based on availability of mice and the capacity to process samples within a given time. After the first experiment, a Power Analysis was conducted to determine subsequent group sizes. All mice were of the C57BL/6J background, except for outbred CD-1 mice. All mice were healthy at the time of infection and were housed in microisolator cages and provided chow, water, and bedding. No mice were administered antibiotics or maintained on water with antibiotics. Experimental groups were littermates of the same sex that were randomly assigned to experimental groups. For experiments with mice deficient in *Ifnar* and *Ifngr*, mice were immediately euthanized if they exhibited severe degree of infection, as defined by a core body temperature dropping below 90˚ F or lethargy that prevented normal movement.

Mouse genotyping

Tlr4$^{-/-}$ [48], *Ifnar*$^{-/-}$ [49], *Ifngr*$^{-/-}$ [50], *Ifnar*$^{-/-}$*Ifngr*$^{-/-}$ and WT C57BL/6J mice were previously described and originally obtained from Jackson Laboratories. CD-1 mice were obtained from Charles River. For genotyping, ear clips were boiled for 15 min in 60 µl of 25 mM NaOH, quenched with 10 µl Tris-HCl pH 5.5, and 2 µl of lysate was used for PCR using SapphireAMP (Takara, RR350) and gene-specific primers. Primers used were: *Ifnar* forward (F): CAACATACTACAACGACCAAGTGTG; *Ifnar* WT reverse (R): AACAAACCCCCAAACCCCAG; *Ifnar*$^{-/-}$ R: ATCTGGACGAAGAGCATCAGG; *Ifngr* (F): CTC GTG CTT TAC GGT ATC GC; *Ifngr* (R): TCG CTT TCC AGC TGA TGT ACT; WT *Tlr4* (F): CACCTGATACTTAATGCTGGCTGTAAAAAG; WT *Tlr4* (R): GGTTTAGGCCCCAGAGTTTTGTTCTTCTCA; *Tlr4*$^{-/-}$ (F): TGTTGCCCTTCAGTCACAGAGACTCTG; and *Tlr4*$^{-/-}$ (R): TGTTGGGTCGTTTGTTCGGATCCGTCG.

Mouse infections

For mouse infections, *R. parkeri* was prepared by diluting 30%-prep bacteria into cold sterile PBS on ice. Bacterial suspensions were kept on ice during injections. For i.d. infections, mice were anaesthetized with 2.5% isoflurane via inhalation. The right flank of each mouse was shaved with a hair trimmer (Braintree CLP-41590), wiped with 70% ethanol, and 50 µl of bacterial suspension in PBS was injected intradermally using a 30.5-gauge needle. Mice were monitored for ~3 min until they were fully

awake. No adverse effects were recorded from anesthesia. For i.v. infections, mice were exposed to a heat lamp while in their cages for approximately 5 min and then each mouse was moved to a mouse restrainer (Braintree, TB-150 STD). The tail was sterilized with 70% ethanol, and 200 µl of bacterial suspension in sterile PBS was injected using 30.5-gauge needles into the lateral tail vein. Body temperatures were monitored using a rodent rectal thermometer (BrainTree Scientific, RET-3).

For fluorescent dextran experiments, mice were intravenously injected with 150 µl of 10 kDa dextran conjugated with Alexa Fluor 680 (D34680; Thermo Fisher Scientific) at a concentration of 1 mg/ml in sterile PBS[34]. As a negative control, mice with no *R. parkeri* infection were injected with fluorescent dextran. As an additional negative control, uninfected mice were injected intravenously with PBS instead of fluorescent dextran. At 2 h post-injection, mice were euthanized with CO_2 and cervical dislocation, doused with 70% ethanol, and skin surrounding the injection site (approximately 2 cm in each direction) was removed. Connective tissue between the skin and peritoneum was removed, and skin was placed hair-side-up on a 15 cm Petri dish. Skin was imaged with an LI-COR Odyssey CLx (LI-COR Biosciences), and fluorescence was quantified using ImageStudioLite v5.2.5. The skin from mice with no injected fluorescent dextran was used as the background measurement. Skin from mice injected with fluorescent dextran but no *R. parkeri* was normalized to an arbitrary number (100), and *R. parkeri*-infected samples were normalized to this value (*R. parkeri*-infected / uninfected X 100). The number of pixels at the injection site area was maintained across experiments (7,800 for small area and 80,000 for the large area).

All mice in this study were monitored daily for clinical signs of disease throughout the course of infection, such as hunched posture, lethargy, scruffed fur, paralysis, facial edema, and lesions on the skin of the flank and tail. If any such symptoms were observed, mice were monitored for changes in body weight and temperature. If a mouse displayed severe signs of infection, as defined by a reduction in body temperature below 90˚F or an inability to move normally, the animal was immediately and humanely euthanized using CO_2 followed by cervical dislocation, according to IACUC-approved procedures. Pictures of skin and tail lesions were obtained with permission from the Animal Care and Use Committee Chair and the Office of Laboratory and Animal Care. Pictures were captured with an Apple iPhone 8, software v13.3.1.

For harvesting spleens and livers, mice were euthanized at the indicated pre-determined times and doused with ethanol. Mouse organs were extracted and deposited into 50 ml conical tubes containing 4 ml sterile cold PBS for the spleen and 8 ml PBS for the liver. Organs were kept on ice and were homogenized for ~10 s using an immersion homogenizer (Fisher, Polytron PT 2500E) at 22,000 r.p.m. Organ homogenates were spun at 290*g* for 5 min to pellet the cell debris (Eppendorf 5810R centrifuge). 20 µl of organ homogenates were then serial diluted into 12-well plates containing confluent Vero cells. The plates were then spun at 260*g* for 5 min at room temperature (Eppendorf 5810R centrifuge) and incubated at 33˚C. To reduce the possibility of contamination, organ homogenates were plated in duplicate and the second replicate was treated with 50 µg/ml carbenicillin (Sigma) and 200 µg/ml amphotericin B (Gibco). The next day, at approximately 16 h.p.i., the cells were gently washed by replacing the existing media with 1 ml DMEM containing 2% FBS (GemCell). The media were then aspirated and replaced with 2 ml/well of DMEM containing 0.7% agarose, 5% FBS, and 200 µg/ml amphotericin B. When plaques were visible at 6 d.p.i., 1 ml of DMEM containing 0.7% agarose, 1% FBS, and 2.5% neutral red (Sigma) was added to each well, and plaques were counted at 24 h.p.i.

Statistical analysis

Statistical parameters and significance are reported in the figure legends. For comparing two sets of data, a two-tailed Student's T test was performed. For comparing two sets of *in vivo* p.f.u. data, Mann-Whitney *U* tests were used. For comparing two survival curves, log-rank (Mantel-Cox) tests were used. For comparing curves of two samples (mouse health, weight, and temperature), two-way ANOVAs were used. For two-way ANOVAs, if a mouse was euthanized prior to the statistical endpoint, the final value that was recorded for the mouse was repeated until the statistical endpoint. For two-way ANOVAs, if a measurement was not recorded for a timepoint, the difference between values at adjacent time points was used. Data were determined to be statistically significant when $P<0.05$. Asterisks denote statistical significance as: *$P<0.05$; **$P<0.01$; ***$P<0.001$; ****$P<0.0001$, compared to indicated controls. Error bars indicate standard deviation (SD) or, for averages of mouse

health/temperature/weight, standard error of the mean (SEM). All other graphical representations are described in the figure legends. Statistical analyses were performed using GraphPad PRISM v7.0.

Data availability

WT and *ompB* mutant *R. parkeri* were authenticated by whole genome sequencing and are available in the NCBI Trace and Short-Read Archive; Sequence Read Archive (SRA), accession numbers: SRX4401164 (WT) and SRX4401167 (*ompB*::Tn^{STOP}).

Competing interests

The authors declare no competing interests.

Author contributions

T.P.B. performed and analyzed experiments. C.J.T., P.E., D.R.G., and D.A.E. contributed to performing experiments and provided reagents. T.P.B. wrote the original draft of this manuscript with guidance from M.D.W. Critical reading and edits of the manuscript were provided by C.J.T., P.E., and M.D.W. Supervision was provided by T.P.B. and M.D.W.

Acknowledgements

We thank Neil Fisher for editing this manuscript. P.E. was supported by postdoctoral fellowships from the Sweden-America Foundation. M.D.W. was supported by NIH/NIAID grants R01AI109044 and R21AI138550. D.R.G., D.A.E., and E.H. were partially supported by NIH/NIAID grant R01 AI24493 (E.H.).

Bibliography

1. Bonell, A., Lubell, Y., Newton, P. N., Crump, J. A. & Paris, D. H. Estimating the burden of scrub typhus: A systematic review. *PLoS Negl. Trop. Dis.* **11**, e0005838 (2017).
2. Fang, R., Blanton, L. S. & Walker, D. H. Rickettsiae as Emerging Infectious Agents. *Clinics in Laboratory Medicine* **37**, 383–400 (2017).
3. Sahni, A., Fang, R., Sahni, S. K. & Walker, D. H. Pathogenesis of Rickettsial Diseases: Pathogenic and Immune Mechanisms of an Endotheliotropic Infection. *Annu. Rev. Pathol. Mech. Dis.* **14**, 127–152 (2019).
4. Grasperge, B. J. *et al.* Susceptibility of inbred mice to Rickettsia parkeri. *Infect. Immun.* **80**, 1846–1852 (2012).
5. Sunyakumthorn, P. *et al.* An Intradermal Inoculation Model of Scrub Typhus in Swiss CD-1 Mice Demonstrates More Rapid Dissemination of Virulent Strains of Orientia tsutsugamushi. *PLoS One* **8**, (2013).
6. Osterloh, A. Immune response against rickettsiae: lessons from murine infection models. *Med. Microbiol. Immunol.* **206**, 403–417 (2017).
7. Paddock, C. D. *et al.* Rickettsia parkeri Rickettsiosis and Its Clinical Distinction from Rocky Mountain Spotted Fever . *Clin. Infect. Dis.* **47**, 1188–1196 (2008).
8. Roux, V. & Raoult, D. Phylogenetic analysis of members of the genus Rickettsia using the gene encoding the outer-membrane protein rOmpB (ompB). *Int. J. Syst. Evol. Microbiol.* **50**, 1449–1455 (2000).
9. Goddard, J. Historical and recent evidence for close relationships among Rickettsia parkeri, R. conorii, R. africae, and R. sibirica: Implications for rickettsial taxonomy. *J. Vector Ecol.* **34**, 238–242 (2009).
10. Reed, S. C. O., Lamason, R. L., Risca, V. I., Abernathy, E. & Welch, M. D. Rickettsia actin-based motility occurs in distinct phases mediated by different actin nucleators. *Curr. Biol.* **24**, 98–103 (2014).
11. Lamason, R. L., Kafai, N. M. & Welch, M. D. A streamlined method for transposon mutagenesis of Rickettsia parkeri yields numerous mutations that impact infection. *PLoS One* **13**, 1–12 (2018).
12. Moraru, G. M. *et al.* Evidence of antibodies to spotted fever group rickettsiae in small mammals and quail from Mississippi. *Vector-Borne Zoonotic Dis.* **13**, 1–5 (2013).
13. Moraru, G. M., Goddard, J., Paddock, C. D. & Varela-Stokes, A. Experimental infection of cotton rats and bobwhite quail with Rickettsia parkeri. *Parasites and Vectors* **6**, 1–5 (2013).
14. Krawczak, F. S. *et al.* Ecology of a tick-borne spotted fever in southern Brazil. *Exp. Appl. Acarol.* **70**, 219–229 (2016).
15. Barbieri, A. R. M. *et al.* Species richness and seasonal dynamics of ticks with notes on rickettsial infection in a Natural Park of the Cerrado biome in Brazil. *Ticks Tick. Borne. Dis.* **10**, 442–453 (2019).
16. Londoño, A. F., Mendell, N. L., Walker, D. H. & Bouyer, D. H. A biosafety level-2 dose-dependent lethal mouse model of spotted fever rickettsiosis: Rickettsia parkeri atlantic rainforest strain. *PLoS Negl. Trop. Dis.* **13**, e0007054 (2019).
17. Suwanbongkot, C. *et al.* Spotted fever group rickettsia infection and transmission dynamics in Amblyomma maculatum. *Infect. Immun.* **87**, e00804-18 (2019).
18. Choe, J. E. & Welch, M. D. Actin-based motility of bacterial pathogens: mechanistic diversity and its impact on virulence. *Pathog. Dis.* **74**, ftw099 (2016).
19. Lamason, R. L. & Welch, M. D. Actin-based motility and cell-to-cell spread of bacterial pathogens. *Current Opinion in Microbiology* **35,** 48–57 (2017).
20. Cheng, M. I., Chen, C., Engström, P., Portnoy, D. A. & Mitchell, G. Actin-based motility allows Listeria monocytogenes to avoid autophagy in the macrophage cytosol. *Cell. Microbiol.* **20**, e12854 (2018).
21. Mitchell, G. *et al.* Listeria monocytogenes triggers noncanonical autophagy upon phagocytosis, but avoids subsequent growth-restricting xenophagy. *Proc. Natl. Acad. Sci. U. S. A.* **115**, E210–E217 (2017).

22. Yoshikawa, Y. *et al.* Listeria monocytogenes ActA-mediated escape from autophagic recognition. *Nat. Cell Biol.* **11**, 1233–1240 (2009).
23. Yoshikawa, Y., Ogawa, M., Hain, T., Chakraborty, T. & Sasakawa, C. Listeria monocytogenes ActA is a key player in evading autophagic recognition. *Autophagy* **5**, 1220–1221 (2009).
24. Auerbuch, V., Lenz, L. L. & Portnoy, D. A. Development of a competitive index assay to evaluate the virulence of Listeria monocytogenes actA mutants during primary and secondary infection of mice. *Infect. Immun.* **69**, 5953–5957 (2001).
25. Le Monnier, A. *et al.* ActA is required for crossing of the fetoplacental barrier by Listeria monocytogenes. *Infect. Immun.* **75**, 950–957 (2007).
26. Goossens, P. L., Milon, G. & Bevan, M. Induction of protective CD8+ T lymphocytes by an attenuated listeria monocytogenes actA mutant. *Int. Immunol.* **4**, 1413–1418 (1992).
27. Brundage, R. A., Smith, G. A., Camilli, A., Theriot, J. A. & Portnoy, D. A. Expression and phosphorylation of the Listeria monocytogenes actA protein in mammalian cells. *Proc. Natl. Acad. Sci. U. S. A.* **90**, 11890–11894 (1993).
28. Jeng, R. L. *et al.* A Rickettsia WASP-like protein activates the Arp2/3 complex and mediates actin-based motility. *Cell. Microbiol.* **6**, 761–769 (2004).
29. Kleba, B., Clark, T. R., Lutter, E. I., Ellison, D. W. & Hackstadt, T. Disruption of the Rickettsia rickettsii Sca2 autotransporter inhibits actin-based motility. *Infect. Immun.* **78**, 2240–2247 (2010).
30. Haglund, C. M., Choe, J. E., Skau, C. T., Kovar, D. R. & Welch, M. D. Rickettsia Sca2 is a bacterial formin-like mediator of actin-based motility. *Nat. Cell Biol.* **12**, 1057–1063 (2010).
31. Engström, P. *et al.* Evasion of autophagy mediated by Rickettsia surface protein OmpB is critical for virulence. *Nat. Microbiol.* **4**, 2538–2551 (2019).
32. Harris, E. K. *et al.* Role of Sca2 and RickA in the dissemination of Rickettsia parkeri in Amblyomma maculatum. *Infect. Immun.* **86**, e00123-18 (2018).
33. Burke, T. P. *et al.* Inflammasome-mediated antagonism of type I interferon enhances Rickettsia pathogenesis. *Nat. Microbiol.* **5**, 688–696 (2020).
34. Glasner, D. R. *et al.* Dengue virus NS1 cytokine-independent vascular leak is dependent on endothelial glycocalyx components. *PLoS Pathog.* **13**, 1–22 (2017).
35. Piro, A. S. *et al.* Detection of cytosolic shigella flexneri via a C-terminal triple-arginine motif of GBP1 inhibits actin-based motility. *MBio* **8**, e01979-17 (2017).
36. Rajapakse, S., Weeratunga, P., Sivayoganathan, S. & Fernando, S. D. Clinical manifestations of scrub typhus. *Transactions of the Royal Society of Tropical Medicine and Hygiene* **111,** 43–54 (2017).
37. Kelly, D. J., Foley, D. H. & Richards, A. L. A Spatiotemporal Database to Track Human Scrub Typhus Using the VectorMap Application. *PLoS Neglected Tropical Diseases* **9**, e0004161 (2015).
38. Richards, A. L. & Jiang, J. Scrub typhus: Historic perspective and current status of the worldwide presence of Orientia species. *Tropical Medicine and Infectious Disease* **5**, 49 (2020).
39. Pingen, M., Schmid, M. A., Harris, E. & McKimmie, C. S. Mosquito Biting Modulates Skin Response to Virus Infection. *Trends in Parasitology* **33,** 645–657 (2017).
40. Lestinova, T., Rohousova, I., Sima, M., de Oliveira, C. I. & Volf, P. Insights into the sand fly saliva: Blood-feeding and immune interactions between sand flies, hosts, and Leishmania. *PLoS Negl. Trop. Dis.* **11**, e0005600 (2017).
41. Šimo, L., Kazimirova, M., Richardson, J. & Bonnet, S. I. The essential role of tick salivary glands and saliva in tick feeding and pathogen transmission. *Front. Cell. Infect. Microbiol.* **7**, 281 (2017).
42. Banajee, K. H. *et al.* Amblyomma maculatum feeding augments Rickettsia parkeri infection in a rhesus macaque model: A pilot study. *PLoS One* **10**, 1–20 (2015).
43. Ngwamidiba, M., Blanc, G., Ogata, H., Raoult, D. & Fournier, P. E. Phylogenetic study of Rickettsia species using sequences of the autotransporter protein-encoding gene sca2. *Ann. N. Y. Acad. Sci.* **1063**, 94–99 (2005).
44. Teysseire, N., Chiche-Portiche, C. & Raoult, D. Intracellular movements of Rickettsia conorii adn R. typhi based on actin polymerization. *Res. Microbiol.* **143**, 821–829 (1992).

45. Heinzen, R. A., Hayes, S. F., Peacock, M. G. & Hackstadt, T. Directional actin polymerization associated with spotted fever group Rickettsia infection of Vero cells. *Infect. Immun.* **61**, 1926–1935 (1993).
46. Walker, D. H. The realities of biodefense vaccines against Rickettsia. *Vaccine* **27**, D52-55 (2009).
47. National Research Council. *Guide for the Care and Use of Laboratory Animals. The Biochemical journal.* (2010).
48. Hoshino, K. *et al.* Cutting edge: Toll-like receptor 4 (TLR4)-deficient mice are hyporesponsive to lipopolysaccharide: evidence for TLR4 as the Lps gene product. *J. Immunol.* **162**, 3749–52 (1999).
49. Müller, U. *et al.* Functional role of type I and type II interferons in antiviral defense. *Science.* **264**, 1918–1921 (1994).
50. Huang, S. *et al.* Immune response in mice that lack the interferon-γ receptor. *Science.* **259**, 1742–1745 (1993).